



Large variation of electron-phonon coupling and thermal transport in two-dimensional semimetal triphosphides by modulation doping

Yongchao Rao ¹, C. Y. Zhao,¹ Lei Shen,² and Shenghong Ju ^{1,*}

¹China-UK Low Carbon College, Shanghai Jiao Tong University, Shanghai 201306, China

²Department of Mechanical Engineering, National University of Singapore, Singapore 117575



(Received 16 March 2023; revised 15 June 2023; accepted 20 July 2023; published 8 August 2023)

Recent studies demonstrated that novel two-dimensional (2D) triphosphide semiconductors possess high carrier mobility and show promising thermoelectric performance, but the carrier transport behaviors in 2D semimetal triphosphides have never been elucidated. Herein, using first-principles calculations and Boltzmann transport theory, we reveal that the electron-phonon coupling effect induced by increasing electron concentration can be significant and thus greatly inhibits electron and phonon transport in electron-doped BP₃ and CP₃. The intrinsic heat transport capacity of flexural acoustic phonon modes in the wrinkle structure is largely suppressed because of the strong phonon scatterings, leading to the low phonon thermal conductivities of 1.36 and 5.33 W/(m K) for BP₃ and CP₃ at room temperature, and at high doping level, the enhanced scattering from the electron diminishes the phonon thermal conductivity by 71% and 54%, respectively. Instead, electron thermal conductivity shows nonmonotonic variations with the increase of doping concentration, stemming from the competition between electron-phonon scattering rates and electron group velocity. Notably, the heavy-doping effect induced by strong scattering from the phonon largely suppresses the electron transport and reduces electron thermal conductivity to the magnitude of phonon thermal conductivity. This work sheds light on the electron and phonon transport properties in semimetal triphosphide monolayers and provides an efficient avenue for the modulation of carrier transport by the doping-induced electron-phonon coupling effect.

DOI: [10.1103/PhysRevB.108.085413](https://doi.org/10.1103/PhysRevB.108.085413)

I. INTRODUCTION

Thermal transport underlies the operation of modern devices, from thermoelectric modules to thermal barrier systems to heat-management systems [1–4]. As one of the most appealing fundamental physical problems, efficiently manipulating thermal transport in materials shows enormous practical implications. The interaction between two thermal transport carriers, an electron and a phonon, plays an important role in a variety of physical phenomena, such as the electron-pairing-induced quantum phenomenon of superconductivity [5], Raman spectra [6], and photoemission spectra [7]. With the improved operability in electron heavy doping, the impact of doping-induced electron-phonon coupling (EPC) on thermal transport has been revealed to have a non-negligible effect on phonon thermal conductivity k_{ph} above room temperature [8–10,11]. The miniaturization of electronic devices has caused two-dimensional (2D) thin films to attract surging interest. In such systems, two-dimensionality allows precise control of the carrier density by a gate [12,13]. The doping-tuned EPC effect can effectively control the transport dynamics of charge carriers in 2D systems [14–18]. In addition, due to the intrinsic enough density of states near the Fermi energy, a strong EPC is more likely to occur in 2D metallic materials [19].

As one novel type of 2D material, triphosphide monolayers composed of phosphorus and select elements from groups III, IV, and V, can be easily exfoliated from layered materials. Experimentally, the typical layered materials GeP₃ and SnP₃, possessing puckered honeycomb threefold coordinated structures, were first synthesized in the 1970s [20–22]. Subsequent theoretical studies reported the low cleavage energy of the type of 2D triphosphides, suggesting exfoliation of bulk materials as a viable means for the preparation of mono- and few-layer materials [23–26]. More recent studies demonstrated that several 2D triphosphides show a high thermoelectric figure of merit due to their low k_{ph} [27]. Such a low k_{ph} can be attributed to low acoustic group velocity and strong phonon-phonon (ph-ph) scattering. Moreover, unlike in graphenelike plane structures, the contribution of the flexural acoustic (ZA) mode to the in-plane thermal conductivity in puckered structures is largely suppressed due to the strong ph-ph scattering.

Triggered by these fascinating findings, an obvious question arises: Can the elements of the short period in the periodic table exit in 2D triphosphides, and if they can exit, what properties and applications can be expected? In fact, C-P films have been successfully synthesized using the unbalanced reactive magnetron sputtering approach [28] and the novel carbon-doping technique [29], and the C:P ratio shows a significant effect on the band gap [30]. From the theoretical perspective, Kar *et al.* [31] predicted a route to synthesize CP₃ monolayers through C atom doping into blue phosphorene. Notably, the electron delocalization resulting in

*shenghong.ju@sjtu.edu.cn

the metallic behavior of CP₃ monolayers further motivates us to investigate the EPC effect in 2D semimetal triphosphides. In addition, a BP₃ monolayer analogous to blue phosphorene was reported by Shojaei and Kang using the CALYPSO [32]. Over the past few years, great effort has been made to explore the effect of electron and phonon interactions on thermal transport in 2D semiconductors [14,15,18], the semimetal W₂N₃ [33], and BeN [34] using first-principles calculations. For most of the planar monolayers, the acoustic branches dominate thermal transport. In principle, the high density of charge carriers can efficiently scatter phonons and largely reduce k_{ph} [14,16,18,35]. And the EPC affects k_{ph} in MoS₂ [35] and graphene [16] mainly through the coupling between acoustic phonons and electrons. As for the puckered structures in which the thermal transport contribution from ZA branches is greatly suppressed, the thermal transport considering the effects of EPC remains unexplored. Moreover, in the most reported 2D monolayers, k_{ph} is higher than the electron thermal conductivity k_e , and the modulation of phonon thermal transport has become the focus. However, the modulation of k_e seems to be easier than modulation of k_{ph} by electron doping. An in-depth understanding of EPC on simultaneously regulating the electron and phonon thermal transport in 2D puckered materials in which k_e is bigger than k_{ph} is still missing.

In this work, we conduct comprehensive first-principles calculations to investigate the e -ph scattering effect on the thermal transport of 2D electron-doped semimetal BP₃ and CP₃ for different carrier concentrations. The strong coupling between acoustic flexural phonons in puckered structures results in low k_{ph} , and optical branches dominate phonon transport. At a high doping level, our calculation explicitly shows that the magnitude of e -ph scattering is comparable with the ph-ph scattering in the high-frequency region, thus resulting in the remarkable suppression of phonon transport. k_e displays anomalous variations with the increase of doping concentration due to the competition between e -ph scattering rates and electron group velocity. In heavily doped systems, strong scattering of high-frequency optical phonons on electrons gives rise to the large reduction in k_e to the magnitude of k_{ph} . The Boltzmann transport equation (BTE) calculations reveal effective ways to tune the thermal transport in semimetal BP₃ and CP₃ by doping-induced e -ph scattering.

II. COMPUTATIONAL DETAILS

Density functional theory (DFT) and density functional perturbation theory (DFPT) calculations were carried out with the QUANTUM ESPRESSO package [36]. The Perdew-Burke-Ernzerhof exchange and correlation functionals [37] were employed with the projector augmented wave method. A vacuum thickness of 12 Å was introduced in the simulation domain to eliminate the interactions between different layers. The plane wave cutoff was set to be 100 Ry, and a $15 \times 15 \times 1$ k mesh and a $5 \times 5 \times 1$ q mesh were employed for electronic and DFPT calculations, respectively. The convergence threshold of the electron energy was set to be 10^{-12} Ry. The left panel of Fig. 1 shows the crystal structure of 2D triphosphides, and this phase is similar to blue phosphorene in that two P atoms in the 2×2 hexagonal unit cell of the latter are replaced by two B or C atoms. The optimized lattice parameters are

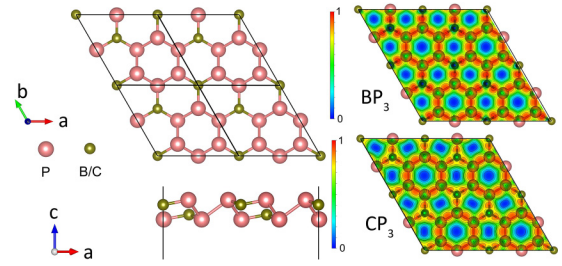


FIG. 1. Top and side views of BP₃ and CP₃ are shown in the left panel. The primitive cell consists of two B/C atoms and six P atoms. The ELF parallel to the (001) plane is shown in the right panel.

6.53 and 6.24 Å for BP₃ and CP₃, respectively, which are consistent with previous first-principles results (6.50 Å for BP₃ [32] and 6.22 Å for CP₃ [31]). By iteratively solving the BTE, the k_{ph} tensor can be written as [38]

$$k_{\text{ph}}^{\alpha\beta} = \frac{1}{N_q V} \sum_{\lambda} \hbar \omega_{\lambda} \frac{\partial n_{\lambda}^0}{\partial T} v_{\lambda}^{\alpha} v_{\lambda}^{\beta} \tau_{\lambda}^{\text{ph}}, \quad (1)$$

where N_q , V , \hbar , ω_{λ} , and n_{λ} are the number of q points in the first Brillouin zone, the volume of the primitive cell, the reduced Planck constant, the frequency of the phonon branch $\lambda = (q, v)$ with polarization v and wave vector q , and the Bose-Einstein distribution function, respectively. v_{λ}^{α} is the projection of the phonon group velocity along the α direction. The relaxation time τ_{λ} , considering both ph-ph scattering and phonon-electron (ph- e) scattering, can be determined by the Matthiessen's rule [38], $1/\tau_{\lambda} = 1/\tau_{\lambda,\text{pp}} + 1/\tau_{\lambda,\text{pe}}$, where $1/\tau_{\lambda,\text{pp}}$ and $1/\tau_{\lambda,\text{pe}}$ are the three-phonon (3ph) scattering rates and ph- e scattering rates, respectively.

For the 3ph scattering process, we adopted the finite-difference method as implemented by THIRDDORDER.PY [39] to calculate third-order interatomic force constants (IFCs) using a $3 \times 3 \times 1$ supercell. The 18th nearest neighbors were included for the calculations of third-order IFCs, and then, the 3ph scattering rates and intrinsic k_{ph} were calculated using SHENGBTE [39] with q points of $60 \times 60 \times 1$ sampling the Brillouin zone. The convergence of k_{ph} with respect to IFC cutoffs and q points sampled in the Brillouin zone is carefully discussed (see Fig. S1 of the Supplemental Material [40] and Refs. [16,23,24,26,34,41–43] therein). $1/\tau_{\lambda,\text{pe}}$ was given by the imaginary part of the phonon self-energy under a complete EPC calculation based on the DFPT and Wannier interpolation techniques. Coarse grids of a $15 \times 15 \times 1$ k mesh and a $5 \times 5 \times 1$ q mesh were interpolated into the dense meshes of a $180 \times 180 \times 1$ k mesh and a $60 \times 60 \times 1$ q mesh through the maximally localized Wannier functions as implemented in the EPW code [44,45]. The Dirac δ functions for electrons and phonons were smeared out by a Gaussian function with widths of 20 and 0.2 meV, respectively. After the total phonon scattering $1/\tau_{\lambda}$ is obtained, k_{ph} considering the ph- e effect was computed by solving equation (1) with an iterative schema. To deal with the thermal transport value of the 2D system, the effective thickness along the vacuum axis was determined by the sum of the thickness of the monolayer sheet and the van der Waals radii of the top and bottom atoms.

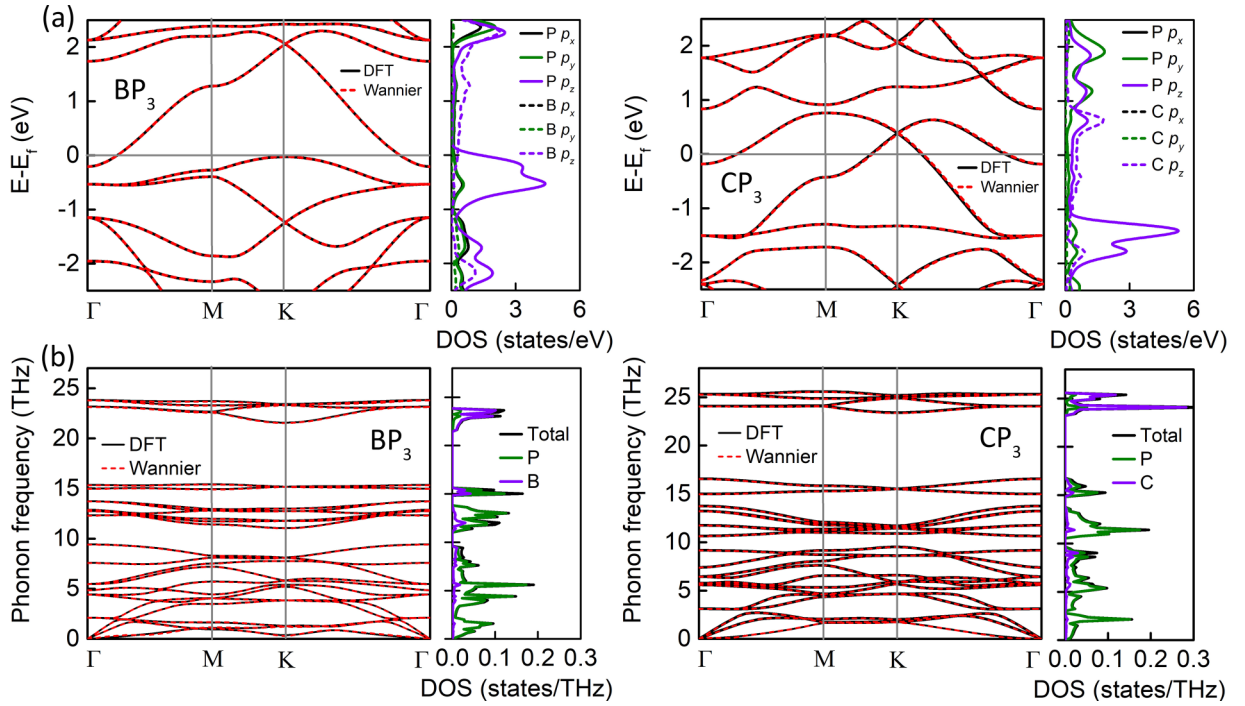


FIG. 2. (a) Electronic band structure and (b) phonon dispersion with the corresponding DOS for BP₃ and CP₃. The black and red lines represent the results calculated by DFT and the Wannier interpolation technique. The electron energy is set to the Fermi energy.

Based on the electronic band structure obtained from Wannier interpolation techniques, k_c and electrical conductivity σ are evaluated by using the electronic BTE and Onsager relations [46]:

$$k_c(\mu, T) = \frac{1}{N_k V} \sum_{n,k} -\frac{(\epsilon_{nk} - \mu)}{T} v_{nk}^2 \tau_{nk}(\mu, T) \times \frac{\partial f_{ED}(\epsilon_{nk}, \mu, T)}{\partial \epsilon} - T S^2(\mu, T) \sigma(\mu, T), \quad (2)$$

$$\sigma(\mu, T) = \frac{1}{N_k V} \sum_{n,k} -e^2 v_{nk}^2 \tau_{nk}(\mu, T) \frac{\partial f_{ED}(\epsilon_{nk}, \mu, T)}{\partial \epsilon} \quad (3)$$

where μ , T , N_k , and e are the chemical potential, the temperature, the total number of k points, and elementary charge, respectively. ϵ_{nk} and v_{nk} are the energy eigenvalue and group velocity of band index n at state k , f_{ED} is the Fermi-Dirac distribution function, and S is the Seebeck coefficient. The electron relaxation time τ_{nk} , limited by e -ph scattering, can be obtained from the imaginary part of the electron self-energy. The change in electron concentration is carried out by a rigid shift of the Fermi level.

III. RESULTS AND DISCUSSION

In the right panel of Fig. 1, we characterize bonding with the electron localization function (ELF). Clearly, the ELF is largest at the center of all P-P and P-B/C bonds, indicating the covalent bonding characteristic of BP₃ and CP₃. Figure 2(a) plots the electronic band structures and projected electron density of states (DOS). Both BP₃ and CP₃ are semimetals, in which electron and hole pockets coexist on the Fermi surface, unlike the semiconductor characteristic in 2D

metal triphosphides [24]. For more insight, we can see that the bands crossing the Fermi level mainly consist of the p_z orbitals of P atoms and the p_z orbitals of B/C atoms. It is concluded that the semimetal behaviors are caused by π types of interaction-induced electron delocalization. The “ π bonds driven semimetal” is in analogy with the “ σ bonds driven metallic” in the MgB₂ superconductor [47].

Figure 2(b) depicts the phonon dispersions and phonon density of states (DOS) of BP₃ and CP₃, and both acoustic and optical modes are primarily contributed by P elements except for the extremely high-frequency optical modes. Two triphosphides show dynamic stability since there are no imaginary phonon modes. The thermal stabilities of 2D BP₃ and CP₃ are confirmed by performing *ab initio* molecular dynamics (AIMD) simulations, as shown in Figs. S5 and S6 of the Supplemental Material [40]. To assess the feasibility of fabrication by mechanical or liquid phase exfoliation, the cleavage energy is calculated by simulating a six-layered model. The calculated cleavage energy is 0.48 and 0.68 J/m² for BP₃ and CP₃, respectively. For comparison, the experimentally reported cleavage energy for graphene is 0.37 J/m² [48], and the DFT-based estimated exfoliation energy for GeP₃ is 1.14 J/m² [24]. In addition, due to the similar morphological structures of 2D triphosphides and blue phosphorene, one possible way to synthesize BP₃ and CP₃ is to dope B/C into blue phosphorene. The feasibility of experimental synthesis of the predicted 2D materials correlates closely with the amount of cohesive energy. The calculated cohesive energy is -4.15 and -4.26 eV/atom for BP₃ and CP₃, respectively, smaller than that of synthesized phosphorene (-3.48 eV/atom [42]) and GeP₃ (-3.34 eV/atom [24]). These results favor further experimental synthesis. Additionally, the highest-frequency modes of BP₃ and CP₃

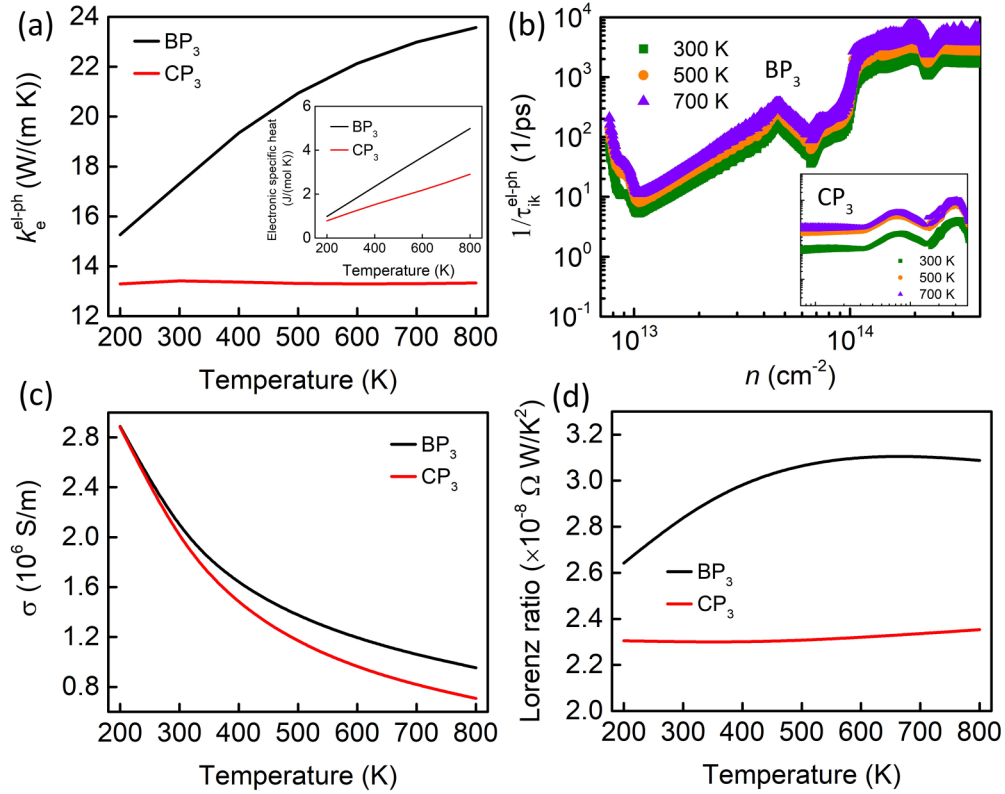


FIG. 3. (a) Electron thermal conductivity k_e , (b) electron scattering rates $1/\tau_{ik}$ at 300, 500, and 700 K, (c) electrical conductivity σ , and (d) the Lorenz ratio versus T for BP₃ and CP₃. The inset in (a) shows how the electronic specific heat varies with T .

appear around 25 THz, which is higher than those of metal triphosphides (14 THz) [27], silicene (17 THz) [49], MoS₂ (14 THz) [50], and phosphorene (13.5 THz) [51], indicating the stronger mechanical strength of bonds in the two triphosphides. Moreover, the frequency of acoustic branches (<2.5 THz) is lower than that in the common 2D materials, including graphene [52], BN [53], transition metal disulfides [50,54], and phosphorene [51], indicating smaller phonon group velocity, as well as the localization of phonon branches with very high 3ph scattering strength, which is a signature of low k_{ph} .

To understand the thermal transport mechanisms in the semimetal BP₃ and CP₃ monolayers, we first examine the separate electron and phonon contributions to thermal conductivity without considering carrier doping. As shown in Fig. 3(a), k_e at 300 K is 17.40 and 13.41 W/(m K) for BP₃ and CP₃, respectively. In semimetal triphosphides, the small density of states at the Fermi level plays non-negligible roles in the electronic contribution to heat conduction. Obviously, k_e of CP₃ is almost temperature independent and is ascribed to the complementary contributions between the decrease in electron relaxation time and the increase in electronic heat capacity with T . However, the value of BP₃ increases with T . As plotted in Fig. 3(b), the electron scattering rates for BP₃ show a slight increase as T increases, which is not comparable to the increasing amplitude in CP₃. In addition, the increase rate of electronic heat capacity for BP₃ is higher than that of CP₃ [inset in Fig. 3(a)]. These features result in the difference in k_e as a function of T between BP₃ and CP₃. We further calculate σ , as illustrated in Fig. 3(c). The magnitude of σ is

on the order of 10^6 S/m, which is significantly smaller than that of typical metals [14,55] and 2D carbon allotropes [56] due to the lower electron DOS near the Fermi level.

The theoretical methods can accurately obtain k_e and k_{ph} , while the experimental techniques are difficult to measure separately. Although some methods have been developed for direct k_{ph} measurements, including the magnetothermal technique [57] and the alloying technique [58], they are limited to the complicated operation process and extremely low temperatures. Benefiting from the easy measurement of electrical conductivity, the approximation $k_{ph} = k_{total} - L\sigma T$ is employed to obtain k_{ph} . Here, the Lorenz ratio is assumed to be the Sommerfeld value $L_0 = 2.44 \times 10^{-8} \Omega W/K^2$ [59]. This approximation is inaccurate when the temperature is far lower than the Debye temperature since L is a chemical-potential- and temperature-dependent quantity because the e -ph scattering rate in the vicinity of the Fermi level is not a constant with respect to the electron energy and temperature. Hence, we also plot L as a function of T in Fig. 3(d). Calculated L in both BP₃ and CP₃ show a trend similar to k_e versus T . The value in BP₃ is bigger than the Sommerfeld value, while the value in CP₃ is smaller. Both L increase with T , which is in agreement with the Bloch-Grüneisen theory [60]. We attribute L large than L_0 to the following reasons. The flat valence band of BP₃ indicates the heavier effective mass of this band compared with the conduction band, resulting in a significant peak of L forming near the Fermi level, and this peak is closer to the valence band. The Fermi level moving to the valence band results in the negative Seebeck coefficient. This sign

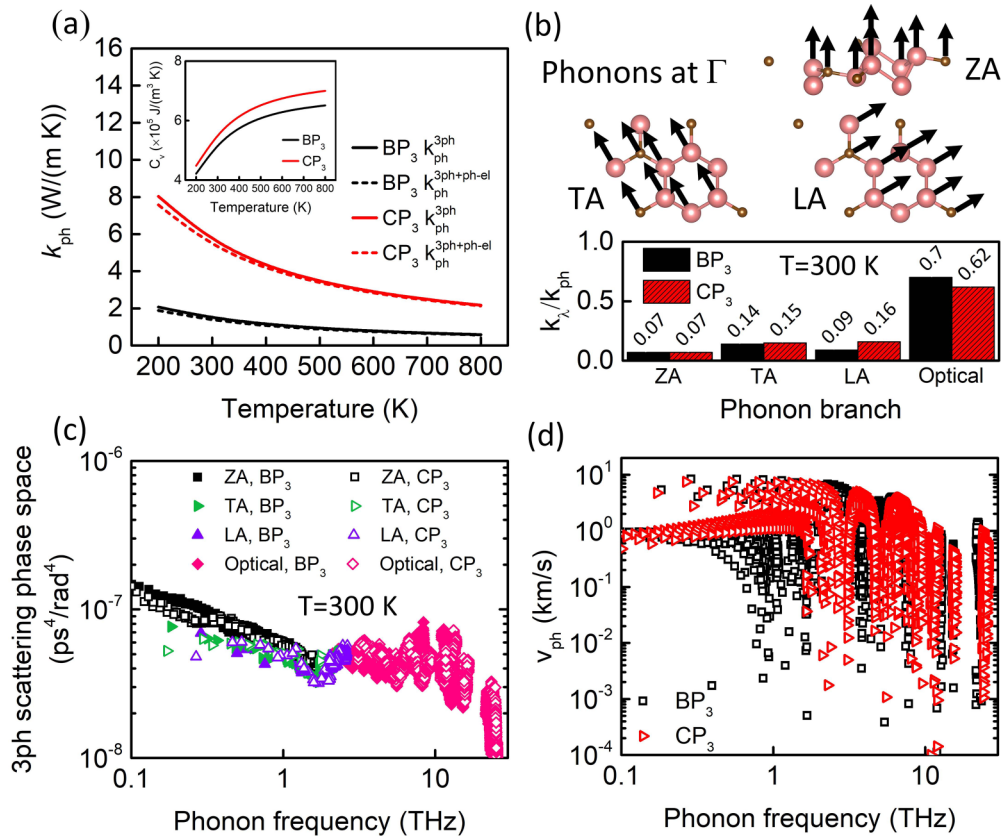


FIG. 4. (a) k_{ph}^{3ph} and $k_{ph}^{3ph+ph-el}$ versus T ; the inset shows the variation of volumetric heat capacity with T . (b) Vibrational pattern of ZA, TA, and LA phonon modes near the Γ point; the bar chart is the ratio of k_x/k_{ph} at $T = 300$ K. (c) Phase space of 3ph scattering processes at 300 K. (d) Phonon group velocity for undoped BP₃ and CP₃.

change of the Seebeck coefficient will result in simultaneous enhancement of k_e and L [61]. Moreover, both electrons and holes in zero-band BP₃ are easier to excite thermally, which enhances the heat transport, hence resulting in an increased L [62,63].

Next, we discuss the phonon contribution to thermal conductivity. Figure 4(a) explicitly shows the temperature-dependent k_{ph} of the intrinsic systems. k_{ph} follows the normal T^{-1} trend generally. As expected, k_{ph} are only 1.48 and 5.60 W/(m K) at 300 K without considering ph- e scattering for BP₃ and CP₃, respectively. For phosphorenelike compounds with puckered structures, the contribution of the ZA mode for k_{ph} is relatively low due to the strong ph-ph scattering. The contribution from the ZA mode shows differences compared with the atomically flat plane, such as representative graphene [11] and BN [64], in which the ZA mode contributes to most k_{ph} . For quantified insights, Fig. 4(b) depicts the contributions of different phonon branches to k_{ph} at 300 K. The acoustic modes contributing to k_{ph} are indeed smaller than optical modes, and the heat conductance contributed by the ZA mode is the smallest. The above-discussed results can be understood by plotting the intrinsic ph-ph scattering rates, as shown in Figs. 5(e) and 5(f). The phonon modes in the low-frequency range present the larger ph-ph scattering rates, indicating the stronger ph-ph scattering strength and lower phonon lifetime, thus predominately limiting the finite thermal conductivity of acoustic modes. Moreover, the strength of 3ph scattering is also reflected in the inverse of phonon

phase space. We plot the scattering phase space of ZA, TA, LA, and optical branches in Fig. 4(c), confirming the abundant scattering channels of the acoustic modes, especially for the ZA modes. Additionally, the insets in Figs. 4(a) and 4(d) depict the temperature-dependent volumetric heat capacity and phonon group velocity, respectively. The larger volumetric heat capacity in CP₃ is one of the reasons why its k_{ph} is higher than that of BP₃. The group velocities of these two systems above 3 THz show insignificant differences due to the very similar phonon dispersions. However, below 3 THz, the low-lying acoustic branches in BP₃ result in its smaller group velocities. Furthermore, unlike in the metallic carbide [65] and nitride [66] systems, k_{ph} of both undoped BP₃ and CP₃ do not show a significant reduction after we consider the ph- e scattering. To give physical insights, the ph-ph and ph- e scattering rates are comparatively plotted in Figs. 5(e) and 5(f) for BP₃ and CP₃, respectively. We can see that the ph-ph scattering rates are obviously larger than ph- e scattering rates over the whole frequency range, which means the phonon lifetime is dominated by ph-ph scattering in undoped triphosphides.

The atom-thick structure endows 2D materials with a greater possibility to manipulate their properties by doping. We next investigate how electron doping can be used to tune the e -ph interactions and then rationally modulate the thermal transport performance. k_e and k_{ph} for both compounds at 300 K varying with electron doping concentration n are shown in Figs. 5(a) and 5(b). k_e of BP₃ exhibits an unusual nonmonotonic dependence on n , while k_e of CP₃ is insensitive

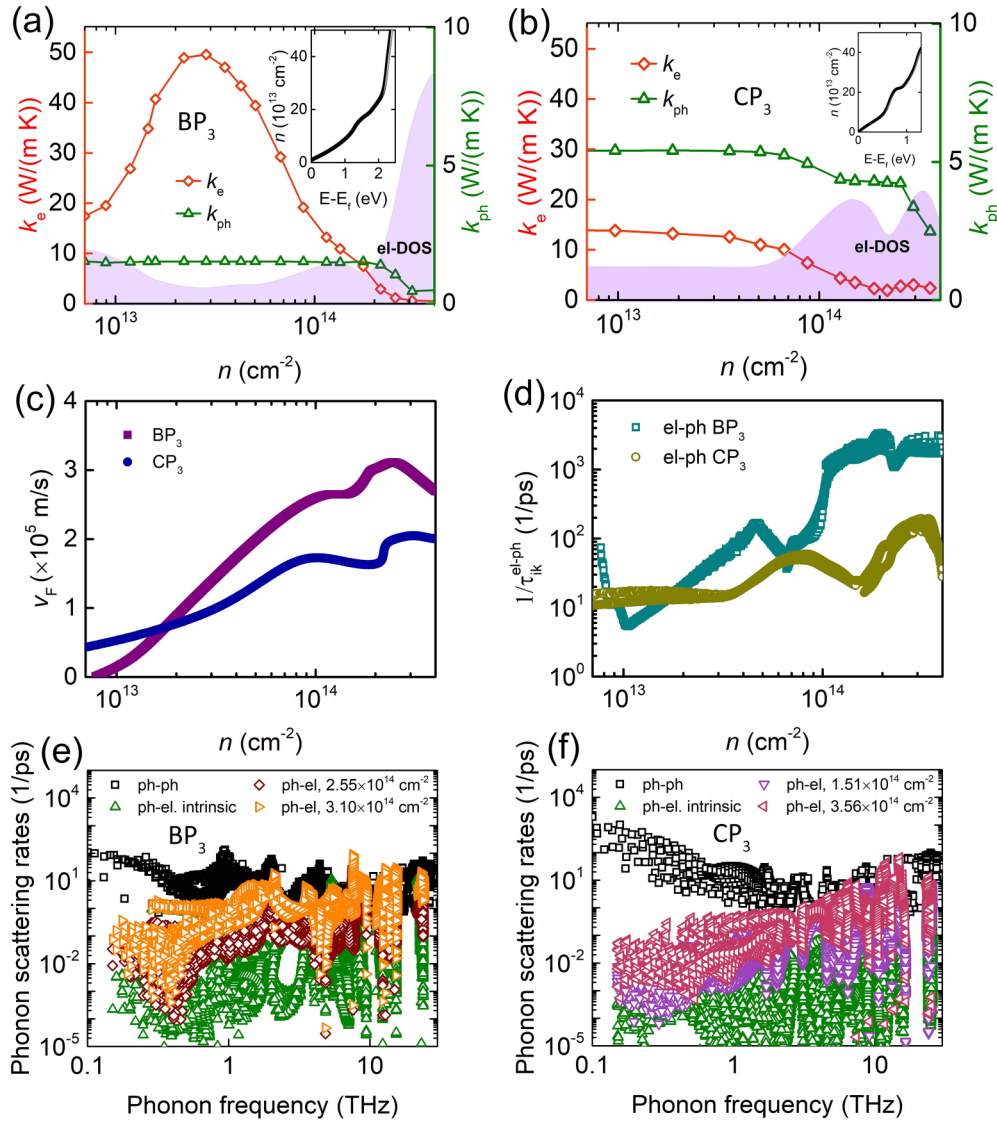


FIG. 5. k_e and k_{ph} as a function of n for electron-doped (a) BP₃ and (b) CP₃. The purple shaded area is the electron DOS, and the corresponding inset shows the variation of n with shifted Fermi energy. (c) v_F and (d) e -ph scattering rates varying with n . The calculated scattering rates of 3ph and ph- e for intrinsic and electron-doped systems with different n for (e) BP₃ and (f) CP₃ at $T = 300$ K.

to n ($< 10^{13}$ cm⁻²) and begins to markedly decrease beyond 10^{13} cm⁻². Compared with the intrinsic system, k_e of BP₃ increases by up to 185% [from 17.40 to 49.58 W/(m K)] at $n = 2.85 \times 10^{13}$ cm⁻², while upon further increasing n up to 4.20×10^{14} cm⁻², k_e reduces to 0.51 W/(m K). k_e of CP₃ reduces from 13.41 to 1.94 W/(m K) at $n = 2.18 \times 10^{14}$ cm⁻². The interaction effect of N_F , v_F , and τ_e on the variation trend of k_e can be qualitatively analyzed by Drude's free electron model, $k_e = \pi^2 k_B^2 T N_F v_F^2 \tau_e / 3$ [65]. Here, N_F is the Fermi DOS highlighted by purple shading in Figs. 5(a) and 5(b). v_F is the Fermi velocity, and τ_e is the electron relaxation time, which are plotted in Figs. 5(c) and 5(d), respectively. At a low doping level, the increased tendency of k_e in BP₃ mainly results from the sharply lowered e -ph scattering rates, as the lowered electron DOS is fully compensated by the enhanced v_F and τ_e . The sharply lowered e -ph scattering rates can be attributed to the decreased electron DOS. When

we continue to increase n ($> 2.85 \times 10^{13}$ cm⁻²), gradually enhanced e -ph interactions result in a minimum k_e despite a surging electron DOS and increased v_F . The fact that k_e of CP₃ shows an insensitive trend with n at a low doping level ($< 3 \times 10^{13}$ cm⁻²) stems from the compensated relationship of the gradually enhanced v_F and decreased τ_e . Further increasing n gives rise to a remarkably enhanced interaction between electrons and phonons and eventually suppresses the electron thermal transport capacity. For both systems, the EPC strength generally increases as n increases. In addition, the electron dominates the overall thermal transport over a wide range ($n < 1.05 \times 10^{14}$ cm⁻²); however, beyond the doping level, the sharp suppression in k_e by largely enhanced EPC leads to k_{ph} surpassing k_e .

k_{ph} in both BP₃ and CP₃ show a monotonous decrease, which becomes more remarkable when the doping level reaches the vicinity of a high electron DOS. The reduction of

k_{ph} in BP₃ and CP₃ can reach 71% at $n = 3.10 \times 10^{14} \text{ cm}^{-2}$ and 54% at $n = 3.56 \times 10^{14} \text{ cm}^{-2}$, respectively. Similar behavior can be observed in heavily doped silicon [8] and 2D Dirac silicene [10] and BeN [34]. We plot the ph- e scattering rates in Figs. 5(e) and 5(f) to quantitatively compare the importance of ph-ph and ph- e scattering events. It can clearly be seen that the ph-ph scattering rates are much higher than ph- e scattering rates in lightly doped systems, which then confirms the insensitivity of k_{ph} to n at the low doping level. However, the ph- e scattering rate becomes comparable at the high doping level. In particular, the high-frequency phonons show remarkable interaction with electrons, which will largely suppress the heat transport capacity of optical modes. As mentioned earlier, optical modes dominate the phonon thermal transport in puckered BP₃ and CP₃. So the decreased trend of k_{ph} at high n is the result of the enhanced electrons scattering on phonons. In total, the EPC can significantly reduce the overall thermal conductivity. This anomalous thermal transport regime by doping-induced strong EPC provides a theoretical basis for experimental detection of the EPC effect on thermal conductivity.

IV. CONCLUSION

By employing first-principles calculations, we systematically predicted k_e and k_{ph} of the 2D semimetals BP₃ and CP₃. The large modulation of thermal conductivity via the

electron-doping-induced EPC effect was demonstrated. The suppression of thermal transport of ZA modes in puckered structures results in low k_{ph} , and electrons dominate the thermal transport. In addition, it was found that the high-frequency optical phonon modes are susceptible to scatter on electrons. When increasing the electron concentration, k_e in BP₃ and CP₃ show different variation trends due to the competition between v_F and τ_e . However, k_{ph} in both systems undergo a monotonic decrease because of the gradually enhanced ph- e interaction with increased n , and their reductions become significant only at a high doping level ($n > 10^{14} \text{ cm}^{-2}$). Furthermore, when $n > 1.05 \times 10^{14} \text{ cm}^{-2}$, k_e of both compounds begin to become lower than k_{ph} due to the sharply enhanced e -ph interaction. Our work sheds light on the intriguing thermal conductivity modulation mechanism in 2D semimetal triphosphides by doping-induced EPC, and the large modulation range of the thermal conductivity indicates its potential application in thermal switching devices.

ACKNOWLEDGMENTS

This work was supported by the National Natural Science Foundation of China (Grant No. 52006134) and the Shanghai Key Fundamental Research via Grant No. 21JC1403300. The computations in this paper were run on the π 2.0 cluster supported by the Center for High Performance Computing at Shanghai Jiao Tong University.

-
- [1] L. E. Bell, Cooling, heating, generating power, and recovering waste heat with thermoelectric systems, *Science* **321**, 1457 (2008).
- [2] A. Liu, H. Xie, Z. Wu, and Y. Wang, Advances and outlook of TE-PCM system: A review, *Carbon Neutrality* **1**, 20 (2022).
- [3] D. R. Clarke and S. R. Phillpot, Thermal barrier coating materials, *Mater. Today* **8**, 22 (2005).
- [4] L. Zhao, K. Roh, S. Kacmoli, K. Al Kurdi, S. Jhulki, S. Barlow, S. R. Marder, C. Gmachl, and B. P. Rand, Thermal management enables bright and stable perovskite light-emitting diodes, *Adv. Mater.* **32**, 2000752 (2020).
- [5] J. Bardeen, L. N. Cooper, and J. R. Schrieffer, Theory of superconductivity, *Phys. Rev.* **108**, 1175 (1957).
- [6] N. Bonini, M. Lazzeri, N. Marzari, and F. Mauri, Phonon Anharmonicities in Graphite and Graphene, *Phys. Rev. Lett.* **99**, 176802 (2007).
- [7] A. Bostwick, T. Ohta, T. Seyller, K. Horn, and E. Rotenberg, Quasiparticle dynamics in graphene, *Nat. Phys.* **3**, 36 (2007).
- [8] B. Liao, B. Qiu, J. Zhou, S. Huberman, K. Esfarjani, and G. Chen, Significant Reduction of Lattice Thermal Conductivity by the Electron-Phonon Interaction in Silicon with High Carrier Concentrations: A First-Principles Study, *Phys. Rev. Lett.* **114**, 115901 (2015).
- [9] T. Wang, Z. Gui, A. Janotti, C. Ni, and P. Karandikar, Strong effect of electron-phonon interaction on the lattice thermal conductivity in 3C-SiC, *Phys. Rev. Mater.* **1**, 034601 (2017).
- [10] T.-H. Liu, J. Zhou, Q. Xu, X. Qian, B. Song, and R. Yang, Significant suppression of phonon transport in polar semiconductors owing to electron-phonon-induced dipole coupling: An effect of breaking centrosymmetry, *Mater. Today Phys.* **22**, 100598 (2022).
- [11] Z. Tong, S. Li, X. Ruan, and H. Bao, Comprehensive first-principles analysis of phonon thermal conductivity and electron-phonon coupling in different metals, *Phys. Rev. B* **100**, 144306 (2019).
- [12] D. K. Efetov and P. Kim, Controlling Electron-Phonon Interactions in Graphene at Ultrahigh Carrier Densities, *Phys. Rev. Lett.* **105**, 256805 (2010).
- [13] C.-L. Wu, H. Yuan, Y. Li, Y. Gong, H. Y. Hwang, and Y. Cui, Gate-induced metal-insulator transition in MoS₂ by solid superionic conductor LaF₃, *Nano Lett.* **18**, 2387 (2018).
- [14] B. Liao, J. Zhou, B. Qiu, M. S. Dresselhaus, and G. Chen, *Ab initio* study of electron-phonon interaction in phosphorene, *Phys. Rev. B* **91**, 235419 (2015).
- [15] S.-Y. Yue, R. Yang, and B. Liao, Controlling thermal conductivity of two-dimensional materials via externally induced phonon-electron interaction, *Phys. Rev. B* **100**, 115408 (2019).
- [16] X. Yang, A. Jena, F. Meng, S. Wen, J. Ma, X. Li, and W. Li, Indirect electron-phonon interaction leading to significant reduction of thermal conductivity in graphene, *Mater. Today Phys.* **18**, 100315 (2021).
- [17] Y. Wu, B. Hou, Y. Chen, J. Cao, H. Shao, Y. Zhang, C. Ma, H. Zhu, R. Zhang, and H. Zhang, Strong electron-phonon coupling influences carrier transport and thermoelectric performances in group-IV/V elemental monolayers, *npj Comput. Mater.* **7**, 145 (2021).
- [18] Z. Zhou, X. Yang, H. Fu, R. Wang, X. Lu, G. Wang, and X. Zhou, Anomalous thermal transport driven by electron-phonon

- coupling in 2D semiconductor h-BP, *Adv. Funct. Mater.* **32**, 2206974 (2022).
- [19] Y. Huang, J. Zhou, G. Wang, and Z. Sun, Abnormally strong electron–phonon scattering induced unprecedented reduction in lattice thermal conductivity of two-dimensional Nb₂C, *J. Am. Chem. Soc.* **141**, 8503 (2019).
- [20] J. Gullman and O. Olofsson, The crystal structure of SnP₃ and a note on the crystal structure of GeP₃, *J. Solid State Chem.* **5**, 441 (1972).
- [21] P. Donohue and H. Young, Synthesis, structure, and superconductivity of new high pressure phases in the systems GeP and GeAs, *J. Solid State Chem.* **1**, 143 (1970).
- [22] L. Häggström, J. Gullman, T. Ericsson, and R. Wäppling, Mössbauer study of tin phosphides, *J. Solid State Chem.* **13**, 204 (1975).
- [23] S. Sun, F. Meng, H. Wang, H. Wang, and Y. Ni, Novel two-dimensional semiconductor SnP₃: High stability, tunable bandgaps and high carrier mobility explored using first-principles calculations, *J. Mater. Chem. A* **6**, 11890 (2018).
- [24] Y. Jing, Y. Ma, Y. Li, and T. Heine, GeP₃: A small indirect band gap 2D crystal with high carrier mobility and strong interlayer quantum confinement, *Nano Lett.* **17**, 1833 (2017).
- [25] L.-P. Feng, A. Li, P.-C. Wang, and Z.-T. Liu, Novel two-dimensional semiconductor SnP₃ with high carrier mobility, good light absorption, and strong interlayer quantum confinement, *J. Phys. Chem. C* **122**, 24359 (2018).
- [26] B. Ghosh, S. Puri, A. Agarwal, and S. Bhowmick, SnP₃: A previously unexplored two-dimensional material, *J. Phys. Chem. C* **122**, 18185 (2018).
- [27] Z. Sun, K. Yuan, Z. Chang, S. Bi, X. Zhang, and D. Tang, Ultra-low thermal conductivity and high thermoelectric performance of two-dimensional triphosphides (InP₃, GaP₃, SbP₃ and SnP₃): A comprehensive first-principles study, *Nanoscale* **12**, 3330 (2020).
- [28] A. Furlan, G. K. Gueorguiev, Z. Czirány, V. Darakchieva, S. Braun, M. Correia, H. Högberg, and L. Hultman, Structure and properties of phosphorus-carbide thin solid films, *Thin Solid Films* **548**, 247 (2013).
- [29] W. C. Tan, Y. Cai, R. J. Ng, L. Huang, X. Feng, G. Zhang, Y.-W. Zhang, C. A. Nijhuis, X. Liu, and K.-W. Ang, Few-layer black phosphorus carbide field-effect transistor via carbon doping, *Adv. Mater.* **29**, 1700503 (2017).
- [30] M. Kuo, P. May, A. Gunn, M. Ashfold, and R. Wild, Studies of phosphorus doped diamond-like carbon films, *Diamond Relat. Mater.* **9**, 1222 (2000).
- [31] M. Kar, R. Sarkar, S. Pal, and P. Sarkar, Two-dimensional CP₃ monolayer and its fluorinated derivative with promising electronic and optical properties: A theoretical study, *Phys. Rev. B* **101**, 195305 (2020).
- [32] F. Shojaei and H. S. Kang, Partially planar BP₃ with high electron mobility as a phosphorene analog, *J. Mater. Chem. C* **5**, 11267 (2017).
- [33] D. Campi, S. Kumari, and N. Marzari, Prediction of phonon-mediated superconductivity with high critical temperature in the two-dimensional topological semimetal W₂N₃, *Nano Lett.* **21**, 3435 (2021).
- [34] Z. Tong, A. Pecchia, C. Yam, H. Bao, T. Dumitrică, and T. Frauenheim, Significant increase of electron thermal conductivity in Dirac semimetal beryllonitrene by doping beyond Van Hove singularity, *Adv. Funct. Mater.* **32**, 2111556 (2022).
- [35] C. Liu, M. Yao, J. Yang, J. Xi, and X. Ke, Strong electron-phonon interaction induced significant reduction in lattice thermal conductivities for single-layer MoS₂ and PtSSe, *Mater. Today Phys.* **15**, 100277 (2020).
- [36] P. Giannozzi *et al.*, Quantum Espresso: A modular and open-source software project for quantum simulations of materials, *J. Phys.: Condens. Matter* **21**, 395502 (2009).
- [37] J. P. Perdew, K. Burke, and M. Ernzerhof, Generalized Gradient Approximation Made Simple, *Phys. Rev. Lett.* **77**, 3865 (1996).
- [38] G. D. Mahan, *Many-Particle Physics* (Springer, New York, 2000).
- [39] W. Li, J. Carrete, N. A. Katcho, and N. Mingo, ShengBTE: A solver of the Boltzmann transport equation for phonons, *Comput. Phys. Commun.* **185**, 1747 (2014).
- [40] See Supplemental Material at <http://link.aps.org/supplemental/10.1103/PhysRevB.108.085413> for details on the calculation methods for the cleavage energy and cohesive energy, the convergence test of q points and IFC cutoffs in phonon thermal conductivity calculations, validation of the Wannier interpolation, partial charge distribution, the electronic band structure of doped systems, electrical conductivity as a function of carrier concentration, and the thermal stability test using *ab initio* molecular dynamics simulations.
- [41] L. Shulenburg, A. D. Baczewski, Z. Zhu, J. Guan, and D. Tomanek, The nature of the interlayer interaction in bulk and few-layer phosphorus, *Nano Lett.* **15**, 8170 (2015).
- [42] Y. Zhang, Z.-F. Wu, P.-F. Gao, D.-Q. Fang, E.-H. Zhang, and S.-L. Zhang, Structural, elastic, electronic, and optical properties of the tricycle-like phosphorene, *Phys. Chem. Chem. Phys.* **19**, 2245 (2017).
- [43] C.-H. Park, N. Bonini, T. Sohier, G. Samsonidze, B. Kozinsky, M. Calandra, F. Mauri, and N. Marzari, Electron–phonon interactions and the intrinsic electrical resistivity of graphene, *Nano Lett.* **14**, 1113 (2014).
- [44] J. Noffsinger, F. Giustino, B. D. Malone, C.-H. Park, S. G. Louie, and M. L. Cohen, Epw: A program for calculating the electron–phonon coupling using maximally localized Wannier functions, *Comput. Phys. Commun.* **181**, 2140 (2010).
- [45] S. Poncé, E. R. Margine, C. Verdi, and F. Giustino, EPW: Electron–phonon coupling, transport and superconducting properties using maximally localized Wannier functions, *Comput. Phys. Commun.* **209**, 116 (2016).
- [46] G. K. Madsen, J. Carrete, and M. J. Verstraete, Boltztrap2, a program for interpolating band structures and calculating semiclassical transport coefficients, *Comput. Phys. Commun.* **231**, 140 (2018).
- [47] J. M. An and W. E. Pickett, Superconductivity of MgB₂: Covalent Bonds Driven Metallic, *Phys. Rev. Lett.* **86**, 4366 (2001).
- [48] R. Zacharia, H. Ulbricht, and T. Hertel, Interlayer cohesive energy of graphite from thermal desorption of polyaromatic hydrocarbons, *Phys. Rev. B* **69**, 155406 (2004).
- [49] S. Cahangirov, M. Topsakal, E. Aktürk, H. Şahin, and S. Ciraci, Two- and One-Dimensional Honeycomb Structures of Silicon and Germanium, *Phys. Rev. Lett.* **102**, 236804 (2009).
- [50] A. Molina-Sanchez and L. Wirtz, Phonons in single-layer and few-layer MoS₂ and WS₂, *Phys. Rev. B* **84**, 155413 (2011).
- [51] G. Qin, Q.-B. Yan, Z. Qin, S.-Y. Yue, M. Hu, and G. Su, Anisotropic intrinsic lattice thermal conductivity of phosphorene from first principles, *Phys. Chem. Chem. Phys.* **17**, 4854 (2015).

- [52] A. K. Geim, Graphene: Status and prospects, *Science* **324**, 1530 (2009).
- [53] K. H. Michel and B. Verberck, Phonon dispersions and piezoelectricity in bulk and multilayers of hexagonal boron nitride, *Phys. Rev. B* **83**, 115328 (2011).
- [54] Z. Zhang, Y. Xie, Y. Ouyang, and Y. Chen, A systematic investigation of thermal conductivities of transition metal dichalcogenides, *Int. J. Heat Mass Transfer* **108**, 417 (2017).
- [55] D. Gall, Electron mean free path in elemental metals, *J. Appl. Phys.* **119**, 085101 (2016).
- [56] Z. Tong, A. Pecchia, C. Yam, T. Dumitrică, and T. Frauenheim, Ultrahigh electron thermal conductivity in T-graphene, biphenylene, and net-graphene, *Adv. Energy Mater.* **12**, 2200657 (2022).
- [57] M. Yao, M. Zebarjadi, and C. P. Opeil, Experimental determination of phonon thermal conductivity and Lorenz ratio of single crystal metals: Al, Cu, and Zn, *J. Appl. Phys.* **122**, 135111 (2017).
- [58] R. Williams, D. Yarbrough, J. Masey, T. Holder, and R. Graves, Experimental determination of the phonon and electron components of the thermal conductivity of bcc iron, *J. Appl. Phys.* **52**, 5167 (1981).
- [59] T. M. Tritt, *Thermal Conductivity: Theory, Properties, and Applications* (Springer, New York, 2005).
- [60] A. Lavasani, D. Bulmash, and S. D. Sarma, Wiedemann-Franz law and Fermi liquids, *Phys. Rev. B* **99**, 085104 (2019).
- [61] M. Thesberg, H. Kosina, and N. Neophytou, On the Lorenz number of multiband materials, *Phys. Rev. B* **95**, 125206 (2017).
- [62] M. T. Pettes, J. Maassen, I. Jo, M. S. Lundstrom, and L. Shi, Effects of surface band bending and scattering on thermoelectric transport in suspended bismuth telluride nanoplates, *Nano Lett.* **13**, 5316 (2013).
- [63] L. Chaput, P. Pécheur, J. Tobola, and H. Scherrer, Transport in doped skutterudites: *Ab initio* electronic structure calculations, *Phys. Rev. B* **72**, 085126 (2005).
- [64] Q. Cai, D. Scullion, W. Gan, A. Falin, P. Cizek, S. Liu, J. H. Edgar, R. Liu, B. C. C. Cowie, E. J. G. Santos, and L. H. Li, Outstanding Thermal Conductivity of Single Atomic Layer Isotope-Modified Boron Nitride, *Phys. Rev. Lett.* **125**, 085902 (2020).
- [65] C. Li, N. K. Ravichandran, L. Lindsay, and D. Broido, Fermi Surface Nesting and Phonon Frequency Gap Drive Anomalous Thermal Transport, *Phys. Rev. Lett.* **121**, 175901 (2018).
- [66] S. Li, A. Wang, Y. Hu, X. Gu, Z. Tong, and H. Bao, Anomalous thermal transport in metallic transition-metal nitrides originated from strong electron-phonon interactions, *Mater. Today Phys.* **15**, 100256 (2020).